MORPHOLOGIC LANDFORMS IN SHOEMAKER AND FAUSTINI LUNAR PERMANENTLY SHADOWED CRATERS. H.M. Brown, M.S. Robinson and A.K. Boyd, Arizona State University, School of Earth and Space Exploration, PO Box 873603, Tempe AZ, 85287-3603 (hbrown6@asu.edu)

Introduction: Lunar permanently shadowed regions (PSRs) harbor cold-trapped volatiles, including water ice, which could provide essential resources for future exploration of the Moon and Solar System [1]. Various remote sensing observations have identified locations in PSRs where volatiles can be thermally stable [2-13] and accumulate over geologic time. Although there have been positive detections of volatiles within PSRs, investigation of true resource potential along with characterization of morphologic landforms that may be indicative of water ice is incomplete.

Here we utilize Lunar Reconnaissance Orbiter Camera (LROC) Narrow Angle Camera (NAC) optical images [14,15] and Lunar Orbiter Laser Altimeter (LOLA) 30 m/pixel slope maps [5,6] to identify and interpret landforms within the two permanently shadowed craters most likely to contain water ice, Shoemaker and Faustini [16]. With a goal to understand geologic processes inside these enigmatic environments, we compare the spatial distribution of positive water frost detections (~1 mm depth) from ultraviolet (UV) albedo [11] and normal albedo 1064 nm reflectance [12] PSR observations and their relation to landforms.

Imaging inside PSRs: Even though PSRs receive no direct solar illumination, they can be imaged with secondary illumination reflected off nearby topographic facets. The NAC can resolve landforms inside PSRs with long integration observations (>10x nominal integration times) at times of maximum secondary illumination [14,17]. Acquisition of NAC PSR observations was refined over several imaging campaigns optimizing the trade-off between signal to noise ratio (SNR) and pixel scale [15,17]. As a result, NAC images best suited to interpret morphological features within PSRs have acceptable SNR (~20 or better; exposure times of 24.2 ms) and relatively coarse pixel scales (10-20 m/pixel).

Resource Potential of PSRs: A patchy veneer of surface frost on crater floors and crater walls was inferred from three different albedo observations (UV, near-IR, and 1064 nm surface albedo [4,11-13,18]). Water ice content ~100 nm thick is estimated to range from 1-10% areal coverage where detected [11], though ice identifications are not always co-located.

Remotely sensed observations from eight datasets in sixty lunar PSRs [16] were used to constrain the locations and quantities of water ice deposits and provide rough estimates of resource potential. From these datasets we conclude that Faustini, Shoemaker, Haworth, Sverdrup, and Cabeus are the most likely resource-rich PSRs [16]. We quantified estimates of resource tonnage in PSRs of interest by finding the areal extent of co-located positive surface frost [11,12] detections. South polar craters Shoemaker and Faustini were found to have the highest potential for water ice and are selected for morphologic analyses.

PSR Landforms: Shoemaker (52 km diameter, 88.03°S, 45.28°E) and Faustini (41 km diameter, 87.15°S, 84.08°E) craters are located in the south circumpolar highlands and are interpreted to have pre-Nectarian formation ages (~4.1-4.2 Ga) and Late-Imbrian (~3.5 Ga) crater retention ages on their floors [19]. Both are flat-floored craters that exhibit geologic features resulting from mass wasting, impact cratering, and tectonism, where each geologic processes has multiple associated landforms (**Table 1**).

Geologic Process	Associated Landforms
Mass wasting	Landslide scarps (head scarps, minor arcuate, lobate, and linear scarps), slump blocks, debris slides, debris flows
Impact cratering	Craters (bowl-shaped, fresh, degraded, asymmetric), secondaries, ejecta blanket material, mound
Tectonism	Lobate scarps

Table 1. Descriptions of mapped morphological features in Shoemaker and Faustini craters.

Results: Landforms identified in Shoemaker and Faustini craters (**Fig. 1**) include slumped material exhibiting head-scarps (**Fig. 2**), impact craters, and lobate scarps on PSR floors. While these landforms are not necessarily unique to PSRs, their formation and rate of occurrence may be associated with temperature and water ice content in PSRs [18].

We find that surface frost identifications (UV albedo and normal albedo [11,12] are positively correlated with mass wasting features (landslide scarps and blocks) and blocky impact ejecta in Shoemaker crater, however in Faustini crater, there is no obvious correlation between landforms at 60-90 m baselines [20] and frost detections. For other resource-rich PSRs [16] (Haworth, Sverdrup, and Cabeus), we find that, at these long baselines, surface frost distribution is also independent of landforms.

Discussion: *Influences on PSR landforms*. Morphology of landforms in PSRs may be a function of thermal stability [11,18]. Recent work suggests [18] that anisothermality within PSRs may lower regolith density. A lower density regolith may have implications for regolith strength and deformation [18].

Previous work interpreting the geology of Shoemaker and Faustini [19] craters found that any water ice that may have been deposited likely had little

influence on modifying the superposed crater population in that time [19].

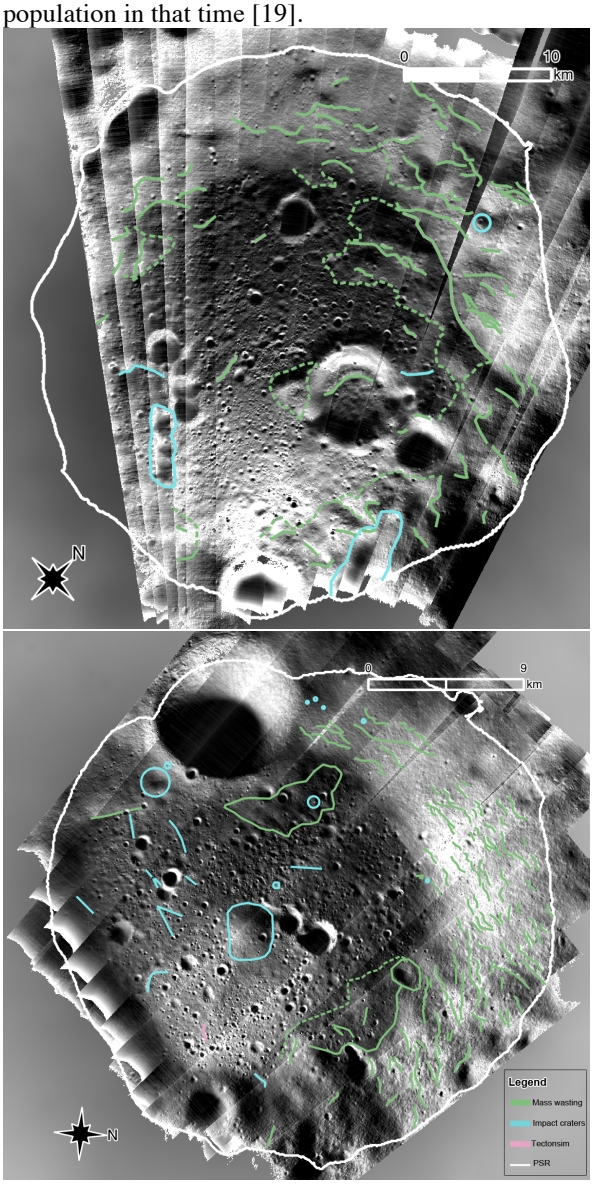

Figure 1. Morphologic maps of Shoemaker (top) and Faustini (bottom) craters. Features are mapped and colored by geologic process (Table 1). Dotted lines indicate boundary extents of slumped material.

Slope Analysis: We compared wall slopes from Faustini and Shoemaker craters to non-ice-bearing craters (Newton B (81.4°S, 343.3°E), Helmholtz F (64.5°S, 60.5°E), Donner T (31.1°S, 94.7°E), and Comrie T (23.0°N, 244.3°E) of similar age and diameter as Shoemaker and Faustini craters. We find that Shoemaker and Faustini craters have slightly steeper median wall slopes (10.2° and 12.3°, respectively) than non-ice-bearing examples (median slopes 5.9°-10.8°). While the difference in wall slope population of each crater is statistically significant, the number of non-ice-bearing craters is low (n=4), and the variation may likely be due to effects other than water ice content and temperature. We also find that depth to diameter (d/D) ratios are comparable between ice-bearing (0.08) and non-ice-bearing (0.06-0.07) craters.

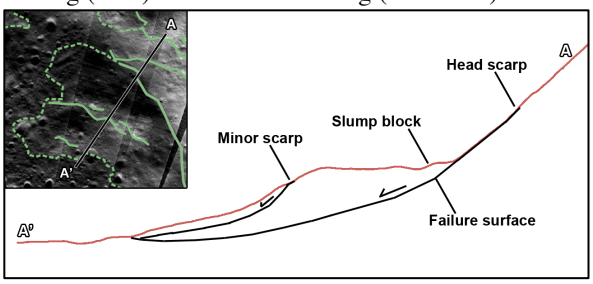

Figure 2. Mass wasting features on the southern facing wall of Shoemaker crater. Topographic profile [20] shown in red. Black lines represent failure surfaces due to slumping.

Conclusion: Characterizing morphological features inside high priority PSRs contributes to future mission planning by enhancing our understanding of the polar regions. Landforms inside two craters likely to host water ice are found to exhibit expressions of geologic processes (mass wasting, impact cratering, and tectonism) as yet indistinguishable from non-ice-bearing craters. Differences in wall slopes are attributed to typical crater variability. Additionally, we found no definitive evidence of permafrost-like landforms or features suggestive of surface frost.

Finer pixel scale and greater SNR imaging may be required to confidently map and interpret smaller landforms that may be indicative of frost and/or water ice buried within the regolith. ShadowCam, a PSR imaging system currently under development will map landforms and albedo variations at high resolution (1.7 m/px) and high SNR (>100) necessary to interpret landforms and enable landed mission planning [21].

Future work will utilize the NAC dataset to characterize landforms in other high priority PSRs [16] and interpret morphology of craters on PSR floors to determine if regolith in ice-bearing PSRs may have stronger geotechnical properties.

References: [1] Arnold J.R. (1979), J. Geophys. Res. 84:5659-5668. [2] Lawrence et al. (2006), J. Geophys. Res., 111.E8. [3] Colaprete et al. (2010), Science, 330, 6003, 463-468 [4] Paige et al. (2010), science, 330, 6003. [5] Smith et al. (2010), Geophys. Res. Lett., 37(18). [6] Mazarico et al. (2011), Icarus, 211(2), 1066-1081. [7] Sanin et al. (2012), J. Geophys. Res., 117.E12. [8] Gladstone et al. (2012), J. Geophys. Res., 117.E12. [9] Spudis et al. (2013), J. Geophys. Res., 118.E10. [10] Glaser et al. (2014), Icarus, 243, 78-90. [11] Hayne et al. (2015), Icarus, 255, 58-69. [12] Fisher et al. (2017), Icarus, 292, 74-85. [13] Li et al. (2018), PNAS., 115(36), 8907-8912. [14] Robinson et al. (2010), SSR, 150.1-4, 81-124. [15] Koeber et al. (2014), LPSC XLV, abs. #2811. [16] Brown et al. (2019), LPSC L, abs. #1054. [17] Cisneros et al. (2017), LPSC XLVIII, abs. #2469. [18] Sefton-Nash et al. 2019, Icarus, Vol 332, 1-13. [19] Tye et al. (2015), Icarus 255, 70-77. [20] Barker et al. (2016), Icarus 273, 346-35. [21] Robinson et al. (2018), LPV, abs. 2087.